Title

Epigenetic heterogeneity shapes the transcriptional landscape of regional microglia

Authors

[1,2,3]Alexander V. Margetts,[1,2]Samara J. Vilca,[1,2]Florence Bourgain-Guglielmetti, [1,2,3]*Luis M. Tuesta

Affiliations

[1]Department of Psychiatry and Behavioral Sciences, University of Miami Miller School of Medicine, Miami, FL 33136

[2]Center for Therapeutic Innovation, University of Miami Miller School of Medicine, Miami, FL 33136

[3]Sylvester Comprehensive Cancer Center, University of Miami Miller School of Medicine, Miami, FL 33136

*Corresponding author at: Department of Psychiatry & Behavioral Sciences, University of Miami Miller School of Medicine, Miami, FL 33136, United States. ltuesta@miami.edu (L.M. Tuesta).

Abstract

Microglia, the innate immune cells in the central nervous system, exhibit distinct transcriptional profiles across brain regions that are important for facilitating their specialized function. There has been recent interest in identifying the epigenetic modifications associated with these distinct transcriptional profiles, as these may improve our understanding of the underlying mechanisms governing the functional specialization of microglia. One obstacle to achieving this goal is the large number of microglia required to obtain a genome-wide profile for a single histone modification. Given the cellular and regional heterogeneity of the brain, this would require pooling many samples which would impede biological applications that are limited by numbers of available animals. To overcome this obstacle, we have adapted a method of chromatin profiling known as Cleavage Under Targets and Tagmentation (CUT&Tag-Direct) to profile histone modifications associated with regional differences in gene expression throughout the brain reward system. Consistent with previous studies, we find that transcriptional profiles of microglia vary by brain region. However, here we report that these regional differences also exhibit transcriptional network signatures specific to each region. Additionally, we find that these region-dependent network signatures are associated with differential deposition of H3K27ac and H3K7me3, and while the H3K27me3 landscape is remarkably stable across brain regions, the H3K27ac landscape is most consistent with the anatomical location of microglia which explain their distinct transcriptional profiles. Altogether, these findings underscore the established role of H3K27me3 in cell fate determination and support the active role of H3K27ac in the dynamic regulation of microglial gene expression. In this study, we report a molecular and computational framework that can be applied to improve our understanding of the role of epigenetic regulation in microglia in both health and disease, using as few as 2,500 cells per histone mark.
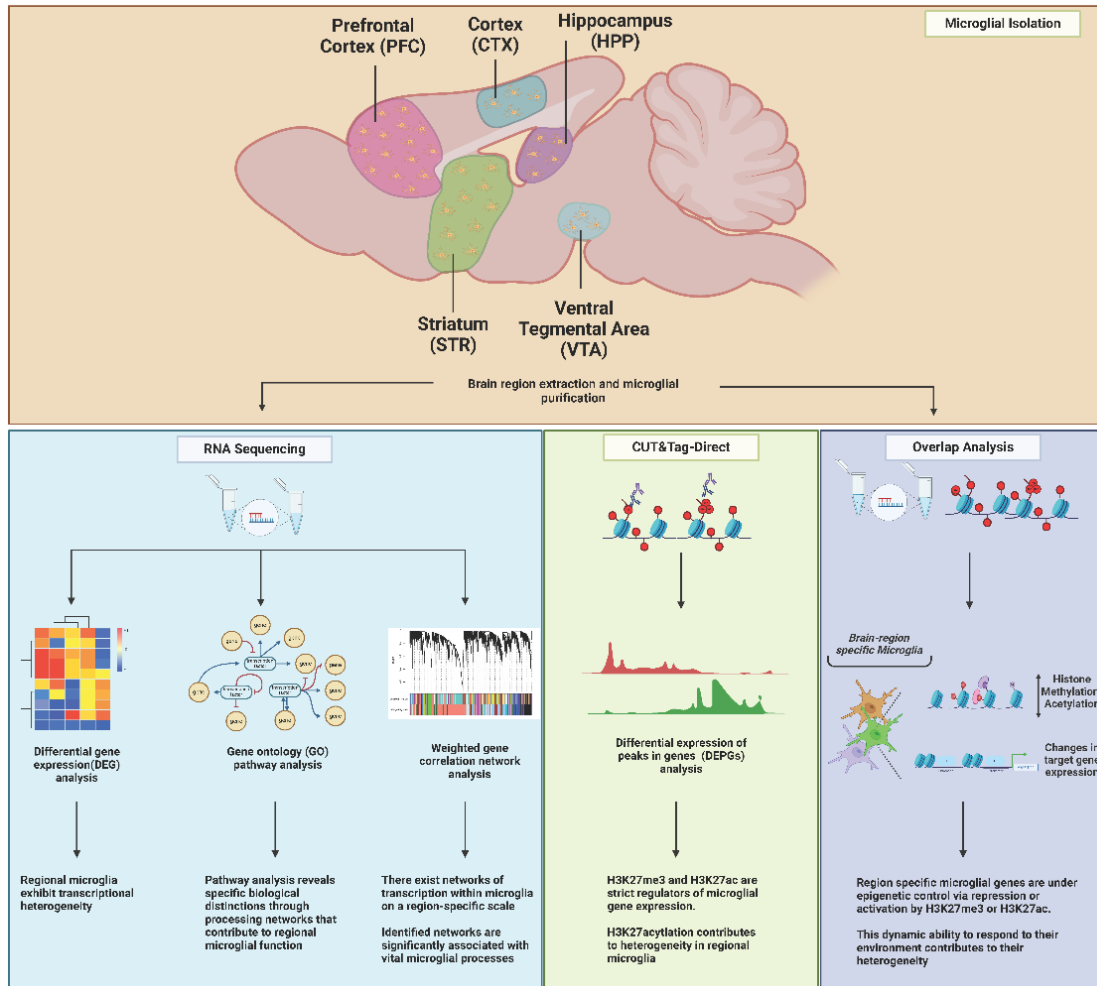
Figure 1. Pipeline of tissue processing and data analysis for the characterization of the microglial transcriptome and epigenome on a regional scale.

Introduction

Microglia are the resident immune cells of the central nervous system (CNS). These cells contribute to various neurological functions throughout the lifespan, such as aiding in neurodevelopment by promoting neurogenesis, cellular differentiation, and shaping neuronal circuits [1, 2]. During adulthood, microglia participate in activity-dependent synaptic pruning, clearing cellular debris from dead and dying cells. Microglia continuously monitor the neural environment, responding to immunological insults or injury by sensing numerous pathogen and damage associated molecules. These reactive microglia are typically characterized by alternate morphologies and secretion of various cytokines (e.g., IL-6, IL-1b, and TNF-a) [1, 2]. Following this initial pro-inflammatory response, microglia then promote tissue repair and resolution of inflammation by releasing anti-inflammatory cytokines, chemokines, and neurotrophic factors [1, 2].

The brain is characterized by its rich cellular heterogeneity, as well as its complex circuitry that contributes to the functional specialization of each brain region. Indeed, microglial gene expression also demonstrates regional heterogeneity. For instance, hindbrain microglia exhibit higher expression of genes associated with clearance activity and immune signaling, while forebrain and midbrain microglia

54 more robustly express genes related to synaptic plasticity and surveillance activity, although to varying
55 levels [3-6]. Specifically, microglia marker genes *Cx3cr1* and *P2ry12* also display regional
56 heterogeneity, showing higher expression in frontal regions compared to midbrain and hindbrain regions
57 [7-9].

58 Interestingly, region-specific transcriptional differences in microglia may be influenced by epigenetic
59 regulation through a suite of transcription factors, epigenetic modifying enzymes, and histone post-
60 translational modifications (PTMs) [3, 10-12]. Indeed, studies suggest the homeostatic microglial
61 transcriptome is regulated by master transcription factor PU.1 [13, 14] and chromatin modifications
62 associated with active promoters (e.g., H3K4me3) and enhancers (e.g., H3K4me1/2 and H3K27ac) [15,
63 16]. Additionally, a recent study demonstrated that striatal and cerebellar microglial function are
64 controlled by polycomb repressive complex 2 (PRC2) [11], which writes the repressive histone mark,
65 H3K27me3. Altogether, these studies suggest microglia fine tune their gene expression to the
66 surrounding neural environment through epigenetic modifications.

67 Indeed, the regions examined in this study are part of, and accessory to, the brain reward system and
68 have been implicated in numerous psychiatric, neurodevelopmental, and neurodegenerative disorders
69 [17-19]. Previous studies have suggested that microglia within these regions may contribute to disease
70 through alteration of their transcriptional landscape [20-23]; however, epigenetic regulation of these
71 cells is less known. Although much effort has been made to characterize the microglial epigenetic
72 landscape in a brain region-specific manner, these efforts have been hampered by technical limitations.
73 For instance, chromatin immunoprecipitation sequencing (ChIP-seq) and assay for transposase-
74 accessible chromatin sequencing (ATAC-seq) have been first-line methods for epigenetic profiling
75 across a broad range of cell types and tissues. In fact, both ATAC-seq and ChIP-seq have been
76 invaluable in enabling the characterization of the microglial epigenome on a global scale [11, 24-31]. In
77 this study we seek to build on these findings by better understanding how these effects can be measured
78 on a regional scale. However, these methods require a significant amount of input (upwards of 500,000
79 cells) to obtain reliable results. Furthermore, while single-cell and single-nucleus sequencing have
80 recently become the preferred methods to examine different cell populations, these are limited by their
81 low sequencing depth. Therefore, a low-input method that retains a high signal-to-noise ratio with
82 minimal sequencing depth (8-10M) is preferable to further examine the epigenetic landscape of brain
83 region-specific microglia. Here, we utilize one such method, Cleavage Under Targets and Tagmentation
84 (CUT&Tag-Direct), that can be used to profile the microglial epigenome from different brain regions
85 with as few as 2,500 cells per histone mark. In this study, we examine the regional differences in naïve
86 microglial gene expression across regions of the brain reward system and associate region-specific
87 transcriptional profiles with repressive (H3K27me3) and permissive (H3K27ac) histone marks. In doing
88 so, we describe a low-input molecular and computational framework, from isolation of primary
89 microglia to preparation of RNA-seq/CUT&Tag-Direct libraries and computational analyses, that can be
90 applied to study region-specific epigenetic and transcriptional changes in microglia both in health and
91 disease models.
92

Results

Region-specific microglia are transcriptionally distinct

93

94

95 We first aimed to determine the transcriptional heterogeneity of microglia by brain region as previously
96 observed [3, 11]. To this end, RNA from purified region-specific microglia were sequenced and
97 differential gene expression analysis confirmed that microglia from the brain regions tested feature
98 distinct transcriptional profiles. More specifically, we found that microglia from the hippocampus (HPP)
99 are the most transcriptionally distinct when compared to somatosensory cortex (CTX), prefrontal cortex
100 (PFC), ventral tegmental area (VTA) and the striatum (STR) (**Fig 2A**). In support, we found numerous
101 differentially expressed genes between the brain regions examined (CTX, PFC, VTA, STR vs HPP:
102 2,681, 4,075, 4,020, 3,723, respectively, padj < 0.01) (**Fig 2B**, **Data S1**). Further, hierarchical clustering
103 using the top differentially expressed genes across all regions shows region-specific transcriptional
104 profiles (**Fig 2C**).
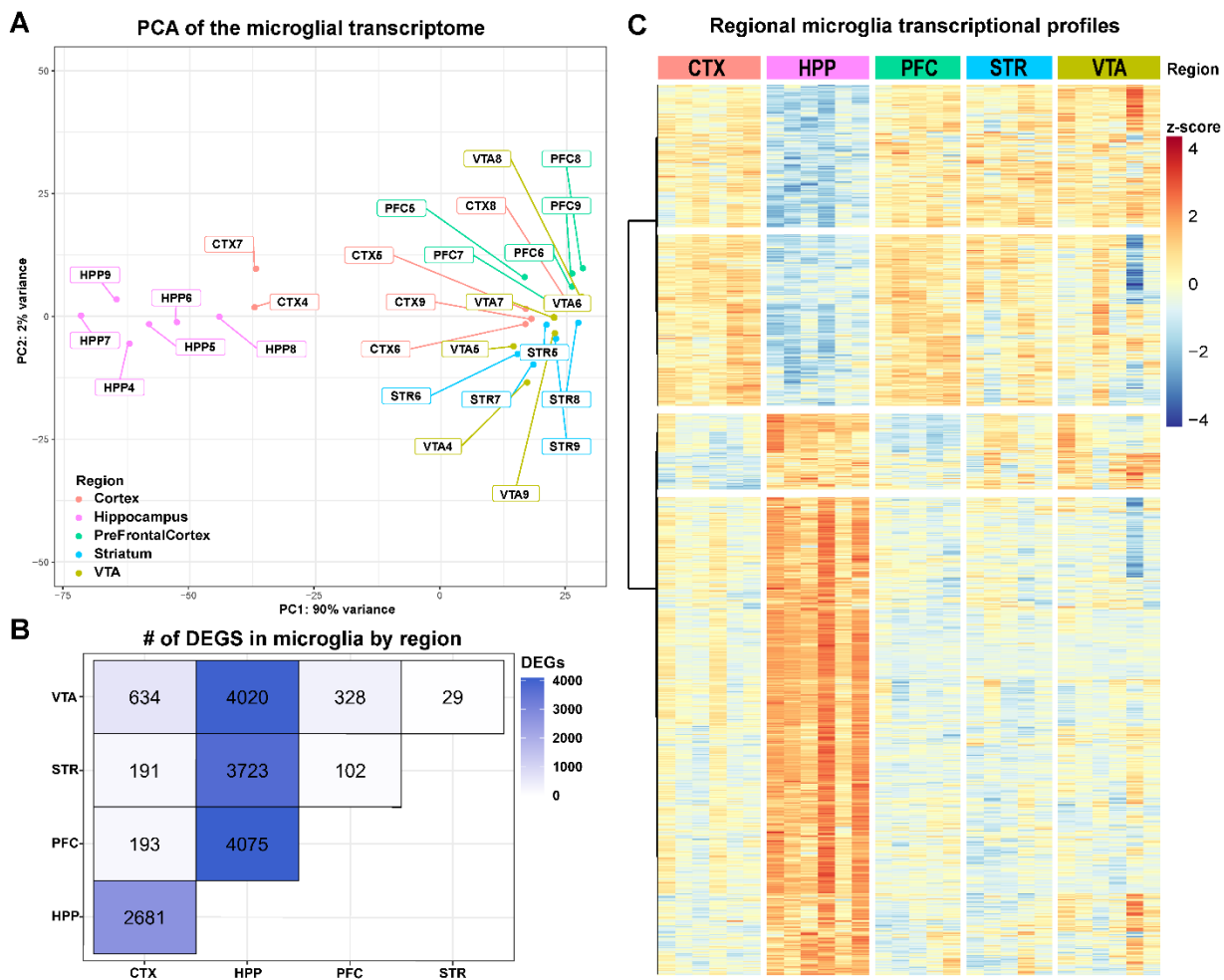
Figure 2. **Microglia exhibit regional transcriptional heterogeneity**. (**A**) Principal components analysis (PCA) indicates variation in baseline transcriptomics in hippocampal (HPP) microglia over other regions. Furthermore, we find (**B**) significant numbers of genes to be differentially expressed between each group in a pairwise comparison (n=5-6, padj <0.01). Of these significant genes we note (**C**) patterns of significant up- and down-regulation of genes in HPP microglia relative to other regions of interest.

105

Pathway analysis reveals biological themes specific to regional microglia

106

107 To better understand the biological relevance of region-specific microglial transcriptomes, gene
108 ontology (GO) pathway analysis was conducted on significantly differentially expressed genes. We
109 found several significantly altered biological pathways which are specific to individual brain regions.
110 Specifically, CTX microglia showed enrichment for pathways related to apical plasma membrane,
111 external encapsulating structure organization, and extracellular structure organization when compared to
112 VTA, as well as cilium processes when compared to STR (**Fig 3A**), suggesting that microglia in the
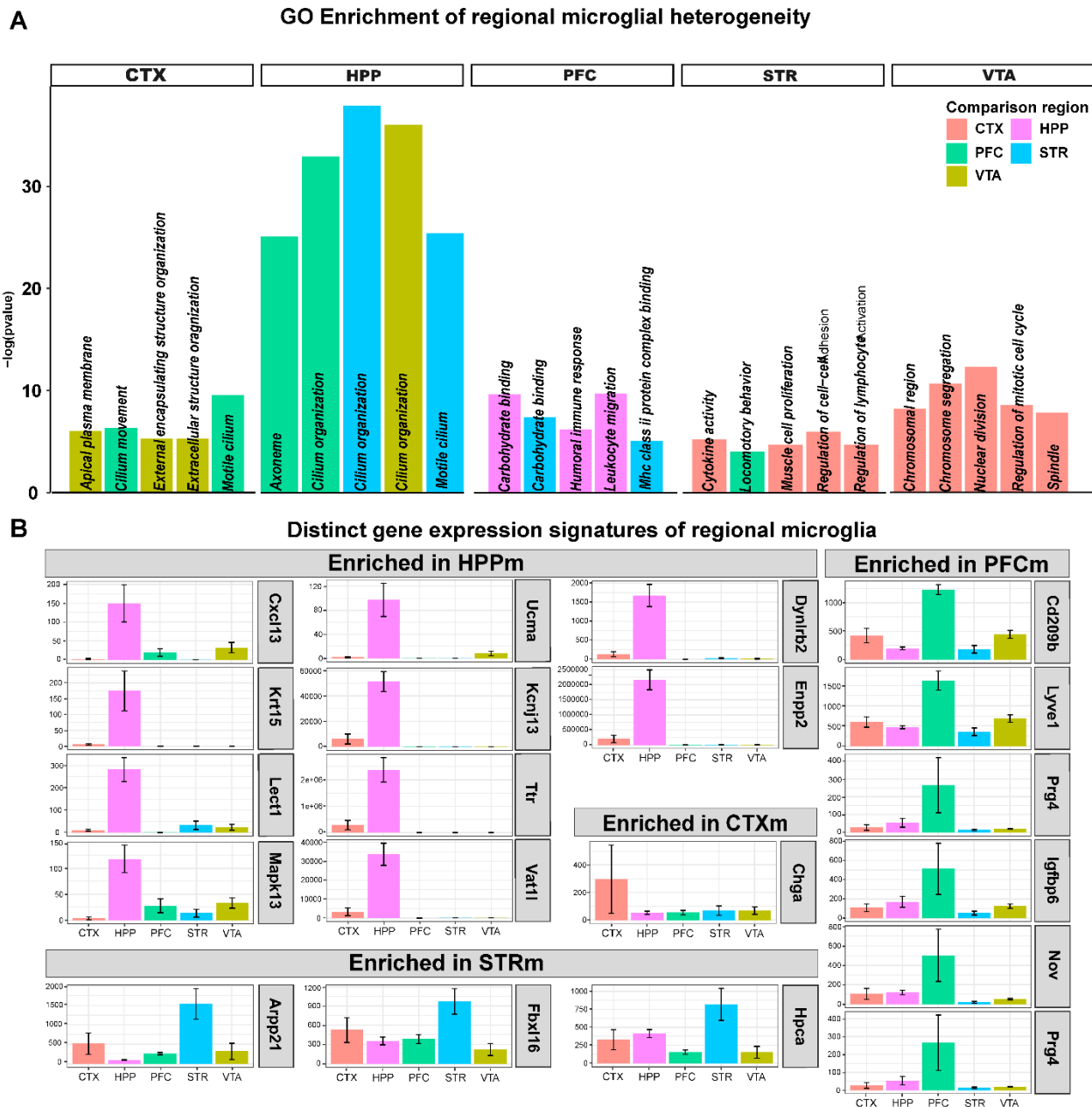
Figure 3. **Transcriptional heterogeneity is linked to region specific gene expression and underlying functional differences**. **(A)** Significantly enriched Gene Ontology (GO) pathways for each region studied (n = 5-7, padj$_{genes}$ < 0.05; padj$_{pathways}$ < 0.01) in a pairwise fashion. **(B)** Normalized gene expression plots highlight significantly enriched genes that are highly expressed in each region (n = 5-7, padj$_{genes}$ < 0.05, Error bars represent SEM).

113 somatosensory cortex may preferentially contribute to extracellular matrix (ECM) formation and overall
114 cortical assembly and structure [32-34]. Additionally, we found microglia from the HPP were enriched
115 for pathways such as axoneme when compared to the PFC, motile cilium when compared to the STR,
116 and overall cilium organization when compared to the PFC, STR, and VTA (**Fig 3A**), indicating
117 hippocampal microglia at baseline conditions may be highly surveilling and secretory compared to other
118 brain regions [35]. Microglia from the PFC were significantly enriched for genes related to carbohydrate
119 binding and leukocyte migration when compared to the HPP, MHC class II protein complex binding
120 when compared to the STR, and humoral immune response when compared to both the STR and HPP
121 (**Fig 3A**), consistent with other studies showing altered cytokine expression in microglia of the frontal
122 cortex [36]. Furthermore, the locomotory behavior pathway was enriched in STR microglia when
123 compared to the PFC (**Fig 3A**), supporting the importance of STR microglia in maintenance of
124 dopaminergic circuitry [6, 37-39]. Additionally, the VTA was enriched for pathways related to
125 chromosomal region, segregation, nuclear division, and regulation of cell cycle when compared to CTX,
126 suggesting that microglia in the VTA may be more proliferative [6], whereas STR microglia were
127 significantly enriched for pathways related to cytokine activity, regulation of cell-cell adhesion, and
128 regulation of lymphocyte activation when compared to CTX microglia (**Fig 3A**). In addition, we find
129 numerous genes that are expressed in a region-specific manner which also underscore these differences
130 in regional microglia (**Fig 3B**).

131 **Weighted gene-network correlation analyses reveal region-specific networks of microglia gene**
132 **expression.**

133 Following differential gene expression analyses, we sought to better characterize the regional
134 differences observed in microglia by identifying modules of expression. To this end, a weighted gene
135 correlation network analysis was conducted and identified 8 modules which show significant mean
136 differential expression across brain regions (**Data S2**). Of these 8 modules, the "salmon" (ME1), "blue"
137 (ME4), "plum" (ME5) and "darkolivegreen" (ME19) modules were selected for further analysis, as they
138 were the most differentially expressed (**Fig 4A**). To understand the biological relevance of these genes,
139 we first filtered the modules for genes with high module membership based on *p*-value correlations and
140 identified hub genes central to each module (**Fig 4C-F**). GO pathway analyses on highly modular genes,
141 those representing the top 1% of modular membership, revealed several differentially expressed
142 pathways between regions (**Fig 4B**). Interestingly, we found that ME1, which is mainly involved in
143 movement and cellular structure, is significantly enriched in hippocampal microglia relative to other
144 regions, while ME5 was significantly depleted in HPP microglia, indicating that GTPase enzymatic
145 activity may be higher in microglia from other regions compared to HPP. Additionally, STR and VTA
146 microglia show enrichment of pathways associated with an immune-activated phenotype including
147 responses to bacteria and stimuli, identified in ME4. Finally, ME19 was slightly enriched in HPP, STR
148 and VTA microglia with higher representation of genes related to cell-cycle phase transition.

149 Taken together, these data support the hypothesis that regional neural microenvironments may regulate
150 microglial gene expression, and that these transcriptional variations enable microglia to execute their
151 unique homeostatic functions across different brain regions. While we identified hippocampal microglia
152 as most transcriptionally distinct from other region-specific microglia, the epigenetic factors that
153 contribute to such heterogeneity remain unclear.
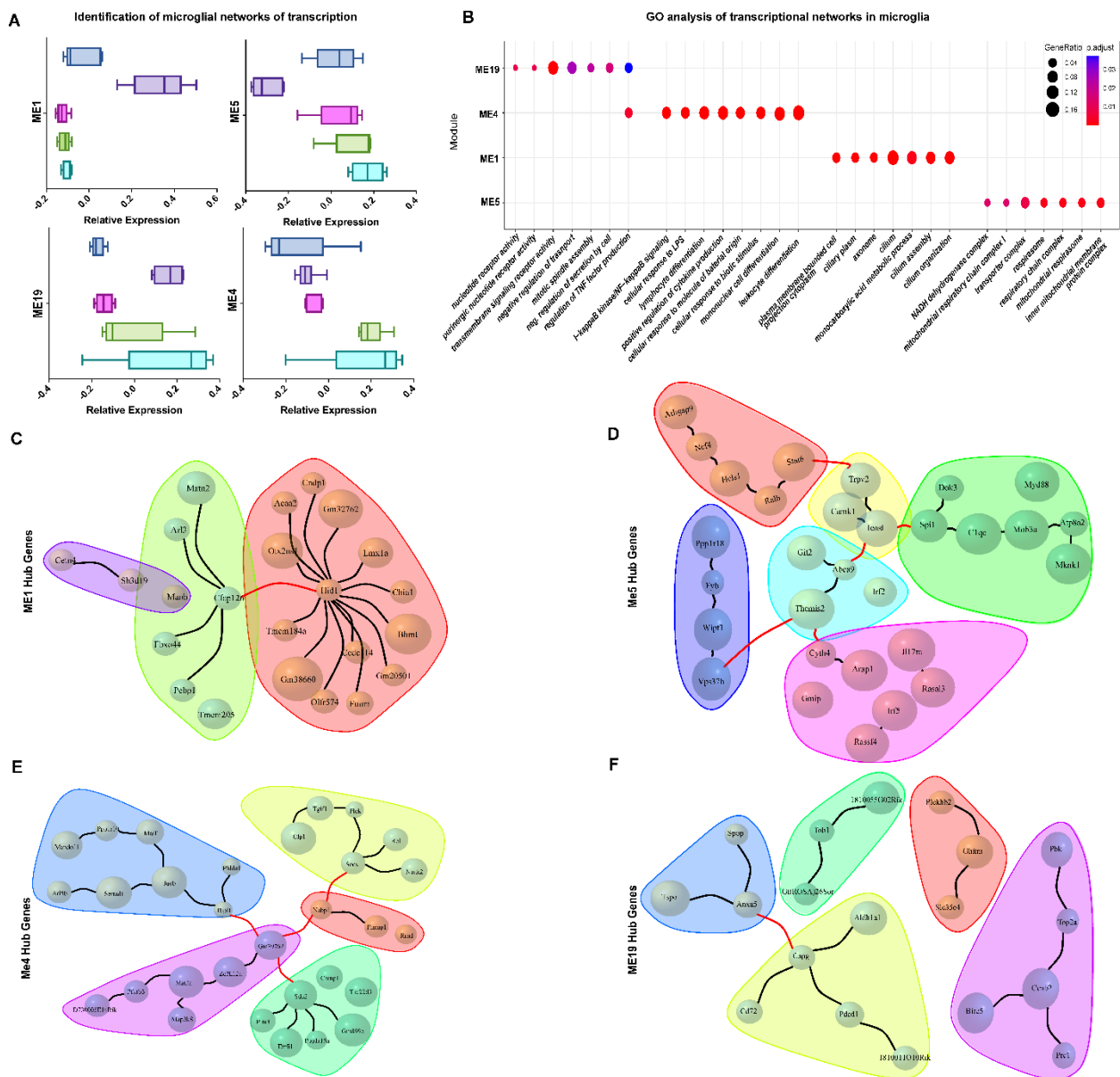
Figure 4. **WGCNA analysis reveals networks of transcription in regional microglia.** **(A)** Significantly differentially expressed modules identified by weighted gene correlation network analysis (limma, ME1: padj < 0.00001; ME5: padj < 0.001; ME19: padj < 0.01; ME4: padj < 0.01) **(B)** GO pathways enriched in highly modular genes for each of the significantly enriched modules (padj < 0.05). Identified hub genes from high modular membership genes (top 1% of genes in each module with module membership *p*-value < 0.05) in the **(C)** ME1 module, **(D)** ME5 Module, **(E)** ME4 Module, **(F)** ME19 Module. (Colors indicate hub genes with closest relationships. Red lines indicate genes with significant connections (Pearson correlation, *p*-value < 0.05))

154

155   **CUT&Tag-Direct enables histone profiling on minimal primary microglial samples.**

156   H3K27me3 is a histone PTM associated with repression and is often found at the transcriptional start

157   site (TSS) and throughout the gene bodies of repressed genes [40, 41]. Conversely, H3K27ac is

158 associated with active transcription and is mainly deposited at, or near the TSS or promoter regions of
159 expressed genes [42]. In order to elucidate the epigenetic regulation of region-specific microglial genes,
160 we conducted CUT&Tag-Direct [43] for H3K27me3 and H3K27ac. Due to the limited number of
161 microglia obtained from tissue extractions, we used CUT&Tag-Direct, a modification of the original
162 protocol for limited cell numbers. To ensure accurate epigenetic mapping, an equal number of designer
163 nucleosomes (dNucs) against a range of histone methylation marks were spiked into each reaction.
164 When compared to other methylation dNucs, the H3K27me3 antibody used for these assays showed
165 high specificity (< 10% non-specific binding) (**Fig S1A**). Indeed, immunohistochemical analysis
166 revealed that the antibodies used were specific and that microglia contain sufficient nuclear material
167 regulated by these marks (**Fig 5A**). Samples yielded robust alignment to the mm10 genome (87% - 97%
168 aligned reads) (**Data S3**). After merging technical replicates, which showed high levels of similarity
169 (**Fig S1B**), peaks were called using SEACR[44], which identified upwards of 150,000 significant peaks
170 in each region for both H3K27me3 and H3K27ac (**Data S3**).

Epigenetic contributions to microglial heterogeneity

172 To determine the contribution of these histone PTMs to transcriptional differences in region-specific
173 microglia, we generated fragment counts within genes related to the histone marks of interest and
174 conducted differential peak deposition analysis using DESeq2. In agreement with previous studies[45],
175 H3K27ac and H3K27me3 are not often simultaneously present at gene promoters (**Fig 5B**).
176 Interestingly, H3K27ac appears to vary by region, suggesting this mark may regulate expression of
177 many genes, whereas H3K27me3 shows a more stable deposition pattern (**Fig S2A**). H3K27me3
178 deposition varied greatly in HPP microglia over other regions, and a majority of significantly differential
179 depositions in genes (DEPGs) appeared in HPP versus STR (1,691 genes containing differential
180 depositions, padj <0.05). Additionally, HPP microglia greatly differ when compared to PFC microglia
181 (756 genes containing differential deposition, padj <0.05). Furthermore, PFC and STR microglia exhibit
182 differential deposition of H3K27me3 when compared to VTA (344, 590 and 151 genes, padj < 0.05)
183 (**Fig 5C, Data S3**). These patterns of H3K27me3 deposition in microglia suggest epigenetic
184 heterogeneity in each region (**Fig 5D**). GO pathway analysis revealed that H3K27me3 deposition is
185 significantly different in genes related to synaptic processes including pre-synapse assembly,
186 organization and structure, as well as GABA receptor complexes when comparing HPP to both STR and
187 PFC microglia (**Fig 5F, Data S3**). Microglia from the VTA exhibit significant differential deposition of
188 H3K27me3 in pathways related to extracellular matrix and basement membrane (vs PFC), actin-filament
189 and methylated histone or protein binding (vs HPP), glial cell proliferation, histone deacetylase binding
190 and multiple differentiation pathways (vs CTX), and actin cytoskeleton (vs STR) (**Fig 5F, Data S3**).

Figure 5. **Differential peak deposition analysis. (A)** Representative immunohistochemical images of mouse HPP microglia, using the microglial marker Iba1 and H3K27me3 (left) and H3K27ac (right) antibodies that were used in CUT&Tag-Direct. **(B)** Representative heatmap of fragments in the TSS or promoter (H3K27ac) or TSS, promoter or exons (H3K27me3) of genes with significantly called peaks (SEACR). Number of significantly differentially deposited peaks in genes for **(C)** H3K27me3 and H3K27ac in a region to region pairwise comparison. Heatmaps of the top differentially deposited peaks in genes for **(D)** H3K27ac and **(E)** H3K27ac (-1.25 < LFC > 1.25, padj <0.05, LfcSE <1). GO pathway analysis results for **(F)** H3K27me3 peaks enriched in genes and **(G)** H3K27ac peaks enriched in genes.

191

192 Unlike H3K27me3, H3K27ac is a transient mark of active gene transcription [42, 46]. Indeed,
193 significant differential deposition of H3K27ac is far more abundant than that of H3K27me3 (**Fig 5C,**
194 **Data S3**). Similar to H3K27me3 depositions, H3K27ac varied greatly in the HPP over other regions.
195 H3K27ac in hippocampal microglia varies greatly when compared to microglia from the CTX, PFC,
196 STR, and VTA (519, 227, 153, 317 genes containing differential deposition, respectively, padj < 0.05).
197 However, the majority of significantly DEPGs are found in the VTA as compared to the CTX (1,670
198 genes containing differential depositions, padj <0.05). Furthermore, when compared to the VTA,
199 microglia from the PFC and STR exhibit differential regulation of 521 and 154 genes by H3K27ac,
200 respectively (padj <0.05). Mirroring H3K27me3, the deposition pattern of H3K27ac in microglia
201 indicates epigenetic regulation of the transcriptional heterogeneity observed across regions (**Fig 5E,**
202 **Data S3**). GO pathway analysis highlights this heterogeneity, as HPP microglial H3K27ac deposition is
203 significantly enriched in genes involved in actin filament and binding as well as extracellular matrix (vs
204 CTX), cell to cell signaling and glial cell migration (vs STR), cell projection and apical plasma
205 membrane (vs VTA), and actin filament related processes (vs PFC) (**Fig 5G, Data S3**). Differential
206 H3K27ac deposition in the VTA compared to the CTX and PFC indicates significant enrichment in
207 genes related to myelination, as well as axon and neuron ensheathment (**Fig 5G, Data S3**).

208 **Correlating regional microglia gene expression with abundant gene expression**

209 To better understand the overall transcriptional regulation of microglial genes by H3K27me3 and
210 H3K27ac, we conducted a gene-overlap analysis. Here, we sub-set gene expression into lowly expressed
211 (FPKM < 1), moderately expressed (FPKM > 1, FPKM <10) and highly expressed (FPKM > 10) and
212 overlapped these with significantly called peaks found at TSS (for both H3K27me3 and H3K27ac) or
213 exonic regions (for H3K27me3) in protein coding genes. By doing so, we found significant overlap of
214 H3K27ac (active transcription) in all regions with both moderately expressed and highly expressed
215 genes. On the other hand, we found significant overlap of H3K27me3 (repression) in all regions with
216 lowly expressed genes (**Fig S2A**). Furthermore, 1960, 1190, 1552, 1609 and 687 lowly expressed genes
217 are significantly correlated with H3K27me3 deposition, while 738, 667, 897, 739, and 749 highly
218 expressed genes are significantly correlated with H3K27ac deposition in the PFC, STR, VTA, HPP and
219 CTX, respectively (**Fig S2B**).

220 To identify the genes contributing to regional heterogeneity in microglia, the gene lists were then filtered
221 to include only genes unique to each region and containing deposition of each histone modification.
222 Remarkably, 151, 117, 267, 173 and 162 highly expressed genes and 226, 215, 270, 279, and 202
223 moderately expressed genes overlap with significantly called peaks for H3K27ac that are unique to the
224 PFC, STR, VTA, HPP and CTX, respectively. Additionally, we found 229, 146, 213, 186 and 194 lowly
225 expressed genes overlap with significantly called peaks for H3K27me3 that are unique to the PFC, STR,
226 VTA, HPP and CTX, respectively (**Fig S2B**). Indeed, while peaks may be present in the promoter-TSS
227 or gene bodies of these region, thereby indicating uniqueness, these results indicate regional specificity
228 of microglial gene expression that is highly correlated with histone PTMs, with the most genes being
229 regulated by H3K27ac in the VTA (**Fig S2B**). While these patterns suggest epigenetic regulation of
230 genes in a region-specific manner, finding the biological relevance of such regulation requires further
231 characterization.

232 **Region-specific epigenetic regulation of microglial genes**
233 We next sought to obtain an overarching understanding of gene regulation via H3K27me3 and H3K7ac
234 in microglia based on neural environments by overlapping DEGs that contain significant deposition of
235 specific histone PTMs. We find a number of significant overlaps when comparing regions (**Fig 6A, C**).
236 Indeed, in agreement with our transcriptomic data, most significant overlaps are found when comparing

Figure 6. **Differential peak deposition analysis. (A)** Venn diagrams showing the number of significant H3K27me3 depositions in genes (DEPGs) (n = 2, padj < 0.05) with significant upregulated genes (DEGs) (n = 2, padj < 0.05) for each regional comparison. (Red numbers indicate overlapping DEPGs and DEGs for each comparison) **(B)** GO analysis dot plots utilizing overlapping genes as input (padj < 0.10) **(C)** Representative IGV plots of CUT&Tag-Direct and RNA-sequencing normalized BigWigs.

237 HPP microglia to other regions. GO analysis of overlapping genes indicates that epigenetic control of
238 genes by H3K27ac in hippocampal microglia are enriched for pathways related to actin regulatory
239 processes, BMP signaling pathway, and kinases (**Fig 6B**). Hippocampal microglia also show
240 significantly downregulated gene expression (due to high H3K27me3 deposition) related to various
241 immune, proliferation and differentiation pathways (**Fig 6B**). These findings highlight the need for this
242 type of analysis, as merging epigenetic and transcriptomic data underscores differences in microglia
243 across the brain.

Discussion

Microglia are the primary immune cells of the CNS and play a key role in development and homeostasis, as well as disease states [47]. Microglial activity largely depends on communication with neurons and other glia, which can induce both transcriptional and epigenetic changes in microglia. While previous research has examined whole-brain changes in microglial transcriptional profiles, recent studies have interrogated these cells in a region-specific manner. A great focus has been placed on the various transcriptional responses of microglia to different stimuli, yet homeostatic transcriptional differences across the brain have only recently been investigated [3]. Furthermore, epigenetic regulation, which can drive transcriptional heterogeneity, has yet to be fully explored in microglia. This may be due, in part, to the inability to obtain sufficient material for both bulk RNA-seq and epigenetic assays from genetically defined cell populations within a single brain region. Our experimental approach, which optimizes CUT&Tag-Direct in conjunction with low-input RNA-seq, enabled us to profile region-specific primary mouse microglia without the need for large numbers of cells or single-cell sequencing techniques that can be burdened by shallow coverages.

Here, we explored the epigenetic regulation of transcriptional heterogeneity in microglia across five brain reward regions in mice (somatosensory cortex, prefrontal cortex, striatum, hippocampus, and ventral tegmental area). This is the first study of its kind to generate both transcriptional and epigenetic data from primary microglia from the same animals. In this study, we found robust gene expression differences in microglia across all five mouse brain regions queried, highlighting their transcriptional diversity (**Fig 2A-C**). We also identified several regionally expressed genes which may contribute to functional differences in microglia (**Fig 3B**). In our data, GO analysis indicated that naïve hippocampal microglia at baseline are enriched for the aforementioned pathways as compared to PFC, STR and VTA microglia (**Fig 3A**), implying microglia in the hippocampus may form cilia to increase their sensing ability and secretory function [35]. Indeed, previous studies have shown that decreased expression of genes related to axoneme assembly and cilium organization pathways in the hippocampus is associated with Alzheimer's Disease and decreased ramifications and impaired sensing in microglia [35, 48]. We also observed that microglia from the VTA express genes reflective of increased proliferation when compared to CTX microglia, which is consistent with previous studies [6]. Overall, profiling transcriptional homeostatic differences in naive microglia will be key to understanding regional variability under experimental or disease conditions.

Furthermore, in order to identify networks of transcription, or gene co-expression, which cannot be identified using DEG analysis, we conducted WGCNA. WGCNA revealed the existence of subsets of genes that share high expression in some regions, while being lowly expressed in others. Importantly, this study identifies four modules of interest that expand our knowledge of microglial transcriptional heterogeneity. Of note, we again find a number of axoneme, and cilium related pathways enriched in the hippocampus versus other regions. We also found that mitosis and numerous immune related pathways are enriched in microglia from the STR and VTA (**Fig 4A-B**), which aligns with previous studies indicating that VTA microglia show a unique reactive phenotype and may be more susceptible to age-related dysfunction [6, 49, 50], as well as other studies that show higher expression of homeostatic and immune surveillance genes in striatal microglia [11]. From this analysis, we also find that microglia from the CTX and PFC share similar expression across almost all modules, generally expressing genes related to transmembrane signaling receptor activity, indicating a more homogeneous population of microglia in these two regions (**Fig 4A**), also consistent with previous studies [3, 6]. While these transcriptional differences have been previously reported, this study sought to further associate these changes with epigenetic modifications.

289 Previously, ChIP-seq and ATAC-seq have been used to characterize microglia on a global scale [10, 11,
290 30, 31], while more recent studies have conducted single-cell RNA-seq and single-cell ATAC-seq to
291 analyze gene expression and chromatin accessibility [51-57]. Unfortunately, the input required to
292 conduct ChIP-sequencing is often insufficient for regional analysis without requiring prohibitive
293 numbers of animals. While ATAC-seq can identify open (active) regions of chromatin, specific histone
294 PTMs cannot be measured. This study establishes a viable methodology for conducting epigenetic
295 profiling on region-specific microglia, a cell population of very limited yield. Indeed, CUT&Tag-Direct
296 yielded robust, high signal-to-noise data and enabled the identification of upwards of 250,000 histone
297 peaks in some samples (**Data S3**), along with high mapping rates and specificity for the marks studied
298 (**Fig S1**). By focusing on two histone PTMs known to regulate gene expression, H3K27ac and
299 H3K27me3, this study identified uniquely regulated genes across specific brain regions in mice (**Fig
300 5B**). Furthermore, as previous studies have shown, we found that H3K27ac and H3K27me3 do not
301 occupy the same promoters and genes simultaneously, due to their opposing effects on gene expression
302 (**Fig 4A**) [45].

303 This study also uncovered that while histone mark deposition varies by region, these align with gene
304 expression (**Fig 5A**). Most of the transcriptional variation in our dataset was due to regional differences
305 in H3K27ac deposition (**Fig S3A**). By conducting RNA-sequencing in conjunction with CUT&Tag-
306 Direct, this study identified region-specific gene expression that is significantly associated with
307 deposition of either H3K27me3 or H3K27ac. Furthermore, by identifying genes that contained
308 significant depositions of H3K27ac or H3K27me3, we were able to correlate this with regional
309 expression of genes (**Fig 5A**). In fact, many genes identified in our WGCNA analysis were found to
310 have reasonable deposition of each mark indicating there may be regulation of these regional
311 transcriptional networks (**Fig S3B**). These overlapping features indicated that the presence of these
312 marks may directly impact gene transcription in a region-specific manner. Indeed, we not only
313 uncovered that *Cx3cr1* and *Tnf-a* contain depositions of these marks, indicating regulation*,* but we found
314 unique genes specific to each region (**Fig 5B**). Given the known role of H3K27me3 in cell fate
315 determination, we were not surprised that there were far fewer H3K27me3-repressed genes that were
316 unique to each region [58]. On the other hand, we found between 17% and 30% of genes that were
317 unique and highly expressed in each region are associated with H3K27ac expression (**Fig 5B**). Taken
318 together, these results suggest that microglial transcriptional heterogeneity is under regulation, at least in
319 part, by deposition of repressive and permissive histone marks in H3K27.
320
321 This study furthers our understanding of epigenetic regulation of regional microglial gene expression by
322 identifying genes containing significant depositions of H3K27ac or H3K27me3, and which were
323 significantly upregulated or significantly downregulated, respectively (**Fig 6A**). Notably, these
324 differences identify hippocampal microglia as being the most heterogeneous relative to the other regions
325 of the brain reward system that we examined. Interestingly, when GO analysis was conducted on these
326 genes, we found that H3K27ac in hippocampal microglia drove expression of genes involved in cellular
327 transport and cellular structure, while increased presence of H3K27me3 in downregulated genes was
328 identified in immune response-related pathways such as B-cell activation and responses to stimuli such
329 as LPS (**Fig 6B**). Further, we note that concomitant decreases in H3K27me3 and increases in H3K27ac
330 can drive differential gene expression of certain genes, such as *Msx1*, across regions (**Fig 6C**). These
331 data suggest that hippocampal microglia may be more homeostatic, with broad deposition of H3K27me3
332 in genes related to immune pathways, while deposition of H3K27ac occurs in genes necessary for
333 surveillance when compared to other regions of the brain reward system.

334 Sex is an important consideration when studying microglia given that neuroimmune system
335 development is regulated by this biological variable [59, 60] and microglial transcriptional profiles have
336 been shown to differ in males and females [3]. Indeed, while we focused on two key post-translational
337 modifications, namely H3K27ac and H3K27me3, there are numerous other epigenetic contributions to
338 transcriptional control in microglia [12]. Further studies focusing on sex differences within and beyond
339 the regions studied here, including additional post-translational histone modifications, will be necessary
340 to more fully understand the contributions of epigenetic diversity to transcriptional regulation of
341 microglial regional heterogeneity.

342 Taken together, these data combine transcriptional and epigenetic datasets from region-specific primary
343 mouse microglia and highlight the molecular heterogeneity that exists in these cells across the brain
344 reward system. Most importantly, this study establishes a methodology for studying the epigenetic and
345 transcriptional changes that occur in cell populations of limited yield. Such populations may be limited
346 by their anatomical location, or by their limited numerical representation relative to functional
347 importance (i.e. dopamine neurons). Furthermore, application of this molecular and computational
348 framework may also be useful for understanding the epigenetic mechanisms that undergird phase, or
349 time-dependent changes in gene expression associated with various psychiatric, neurodegenerative or
350 neoplastic diseases.
351

352 **Materials and Methods**

353 **1. Animals:** Male C57BL/6J mice (12–16-week-old, ~25-30 g; Jackson Laboratories, Bar Harbor, ME;
354 SN: 000664) were housed in the animal facilities at the University of Miami Miller School of Medicine.
355 Mice were maintained on a 12:12 h light/dark cycle and were housed three to five per cage. Animals
356 were provided with food and water *ad-libitum*. All animals were maintained according to National
357 Institutes of Health (NIH) guidelines and Association for Assessment and Accreditation of Laboratory
358 Animal Care (AAALAC) accredited facilities. All experimental protocols were approved by the
359 Institutional Animal Care and Use Committee (IACUC) at the University of Miami Miller School of
360 Medicine.

361 **2. Microglial Isolation:** Mice were anesthetized with isoflurane and perfused through the ascending
362 aorta with 1X phosphate buffer saline (PBS; pH 7.4; ThermoFisher, 10010023) plus heparin (7,500 USP
363 units). Brain regions from 4 mice (**Fig 1**) were dissected and combined, then transported on ice in
364 Hibernate A Medium (Gibco, A1247501). Tissue was then dissociated on the gentleMACS Octo
365 Dissociator (Miltenyi Biotec, #130-096-427) using the Adult Brain Dissociation Kit (Miltenyi Biotec,
366 #130-107-677) according to manufacturer's instructions. All steps after initial dissociation were
367 performed on ice and all tubes were prechilled. The resulting single cell suspension was incubated with
368 anti-mouse CD11b (microglia-specific) magnetic MicroBeads (Miltenyi Biotec, #130–093–634) and
369 microglia were positively selected via column purification (Miltentyi Biotec, #130-042-201). The eluted
370 fraction containing microglia was then centrifuged for 3 min at 600 x g and resuspended in 110 µL of
371 PBS (ThermoFisher, 10010023). 10 µL was reserved for cell counting on the EVE Countess Automated
372 Cell Counter (NanoEntek), and the remaining 100 µL was split: 30 µL for RNA extraction, 70 µL for
373 CUT&Tag-Direct.

374 **3. Brain Perfusion and Fixation:** Mice were anesthetized with isoflurane and perfused through the
375 ascending aorta with 1X phosphate buffer saline (PBS; pH 7.4; ThermoFisher, 10010023) plus heparin
376 (7,500 USP units) (DVR University of Miami), followed by fixation with 4% paraformaldehyde (PFA;

377   Sigma Aldrich, 1003543951) in PBS. Brains were collected, postfixed overnight in 4% PFA, and then
378   stored in 30% sucrose with 0.05% sodium azide (Sigma Aldrich, 1003124924) in PBS. All brains were
379   cut into 35 μm coronal sections on a cryostat, and floating sections were stored in PBS with 0.02%
380   sodium azide at 4°C until processing for immunohistochemistry.

381   **4. Fluorescence Immunolabeling:** Floating sections were processed for fluorescent immunostaining of
382   microglia. Sections were rinsed in PBS and then blocked for 1 hour at room temperature in Blocking
383   Buffer consisting of 10% normal donkey serum (Jackson ImmunoResearch, 017-000-121), 0.5% Triton
384   X-100 (Sigma Aldrich, T8787), and PBS. Thereafter, sections were incubated in primary antibody in
385   Blocking Buffer at 4°C overnight. The primary antibodies used were as follows: goat anti-Iba1 (1:500,
386   NB1001028, Novus Biologicals), rabbit anti-H3K27me3 (1:500, 9733S, Cell Signaling Technology),
387   and rabbit anti-H3K27ac (1:160, 8173, Cell Signaling Technology). On day 2, the sections were rinsed 3
388   times with PBS and incubated with the following secondary antibodies: Alexa 488 donkey anti-goat
389   (1:500, A32814, Invitrogen) and Alexa 568 donkey anti-rabbit (1:500, A10037, Invitrogen). Sections
390   were incubated with secondary antibodies in PBS with 2% normal donkey serum for 2 hours at room
391   temperature in the dark. Next, sections were rinsed 3 times with PBS, mounted on slides with ProLong
392   Diamond Antifade Mountant with DAPI (Invitrogen, P36962) and cover slipped. Images were acquired
393   using the VS120 Olympus slide scanner housed in the University of Miami Miller School of Medicine's
394   Analytical Imaging Core Facility (AICF). Controls included processing the secondary antibodies alone
395   to verify background staining, processing each primary with the secondary antibody to verify laser-
396   specific excitation, checking for autofluorescence in an alternative laser channel with tissue lacking that
397   laser-specific probe, and using sequential scanning. Fluorescent images were viewed in OlyVIA
398   (Olympus, Ver.2.9.1), where only brightness and/or contrast levels were adjusted after acquisition were
399   imposed across the entire image. All antibodies used have been previously validated for the intended
400   applications, as per manufacturer. For all representative images of qualitative data, the immunolabeling
401   experiment was successfully repeated in 3 animals.

402   **5. RNA-seq:** 30 μL of isolated microglia was added to 350 μL RLT plus buffer (Qiagen, 1053393) for
403   extraction and purification of total RNA according to manufacturer's instructions using the Qiagen
404   AllPrep DNA/RNA Mini Kit (Qiagen, 80204). Total RNA input was normalized and NGS libraries were
405   prepared using NEBNext Single Cell/Low Input RNA Library Prep Kit for Illumina (New England
406   BioLabs, E6420S) according to the manufacturer's instructions. Sequencing was performed on an
407   Illumina NovaSeq6000 platform (150x150bp PE) targeting 30 million reads per sample by the
408   University of Miami Center John P. Hussman Institute for Human Genomics sequencing core facility.

409   **6. RNA-seq Analysis**

410   All RNA-seq data used in this study were mapped to the mm10 genome. Prior to mapping, raw RNA-
411   seq datasets were first trimmed using TrimGalore (v.0.6.7) [61] with cutadapt (v.1.18) [62]. Illumina
412   sequence adaptors were removed, the leading and tailing low-quality base-pairs (fewer than 3) were
413   trimmed. Next, reads with a length of at least 20-bp were mapped to the genome using STAR (v.2.7.10a)
414   [63] with the following parameters: –outSAMtype BAM SortedByCoordinate –outSAMunmapped
415   Within –outFilterType BySJout –outSAMattributes NH HI AS NM MD XS –outFilterMultimapNmax
416   20 –outFilterMismatchNoverLmax 0.3 --quantMode TranscriptomeSAM GeneCounts. The resulting
417   bam files were then passed to StringTie (v.2.1.7) [64] to assemble sequenced alignments into estimated
418   transcript and gene count abundance given the Gencode GRCm38 (NCBI) transcriptome assembly.

419 **6.1 Differential Gene Expression Analysis:** The R/Bioconductor DESeq2 (v.1.34.0) [65] package was
420 used to detect the differentially expressed genes between region-specific microglia. Only genes with
421 transcript abundance > 50 across samples, and adjusted *p*-value (padj) < 0.05 were considered as
422 differentially expressed.

423 **6.2 Functional Enrichment Analysis:** The R/Bioconductor clusterProfiler (v.4.2.2) [66, 67] package
424 was used to perform Gene Ontology (GO) analysis. Only the GO terms and pathways with a padj < 0.05
425 following false discovery rate (FDR) correction were considered, with focus given to those showing
426 positive enrichment only (i.e., log_2foldchange (log_2FC) > 1). The R/Bioconductor package rrvgo (v1.6.0)
427 [68] was utilized to reduce GO terms to parent terms for clarity. The associated GO and pathway
428 enrichment plots were generated using the ggplot2 package (v.3.4.2). Heatmaps were generated using
429 the R/Bioconductor package pheatmap (v.1.0.12). All the other plots were generated using the ggplot2
430 package.

431 **6.3 Weighted Gene Co-Expression Analysis (WGCNA):** The R package WGCNA [69] was used to
432 conduct gene co-expression analysis. Briefly, count matrices were loaded into R and normalized using a
433 variance stabilized transformation (VST). Samples were checked for goodness and manual network
434 construction using a bicorrelation, soft thresholding power of 7, a signed-hybrid network and a signed
435 TOM was conducted. The minimum module size was set at 30 genes and modules were merged based
436 on similarity and assigned a color name. The limma package (v.3.50.3) [70] was used to conduct
437 statistical analysis to identify which modules were significantly differentially expressed (padj > 0.05) by
438 brain region based on average expression of all genes in that module following FDR multiple testing
439 correction. Module expression was plotted with ggplot2 (v.3.4.2). Module membership was calculated
440 and the top 1% of most modular genes were selected and GO pathway enrichment was conducted on
441 them using the R/Bioconductor package clusterProfiler (v.4.2.2) [66, 67] against a background
442 containing all genes mapped to relevant modules with an FDR multiple testing correction. Heatmaps
443 were generated using the R/Bioconductor package pheatmap (v.1.0.12) by generating lists of all genes in
444 each module that mapped to significant GO pathways (padj < 0.05).

445 **7. CUT&Tag-Direct:** CUT&Tag-Direct was conducted with minor modifications [43, 71] [71](See
446 CUTAC-V4 at protocols.io).

447 **7.1 Microglial nuclear isolation and preservation:** Isolated microglia from two biological samples
448 (n=2) were nucleated and lightly-cross-linked before slow-freezing. Briefly, 70 µL of isolated microglia
449 were resuspended in 1 mL NE1 buffer (1 mL 1M HEPES-KOH pH 8.0 [ThermoFisher, J63578.AP], 500
450 µL 1M KCl, 12.5 µL 2M spermidine [Sigma Aldrich, 102597490], 500 µL 10% Triton X-100 [Sigma
451 Aldrich, 1003407653], 1 Roche c0mplete Protease Inhibitor EDTA-free [Sigma Aldrich, 04693232001]
452 , and 10 mL glycerol [Sigma Aldrich, G5516-500ML] and 38 mL ddH2O) for 10 minutes on ice with
453 light vortexing. Nuclei were centrifuged (4 minutes at 1300 *x g* at 4°C*)* and supernatant was removed.
454 Isolated nuclei were then lightly crosslinked in 0.1% formaldehyde (5 mL PBS with 31 µL 16%
455 formaldehyde (*w/v*) [ThermoFisher, 28908]) at room temperature for 2 minutes. 300 uL 1.25 M glycine
456 [Thomas Scientific, 762Q84] was used to stop cross-linking and nuclei were centrifuged (4 minutes at
457 1300 *x g* at 4°C) and resuspended in 100 µL Wash Buffer (1 mL 1M HEPES pH 7.5 [ThermoFisher,
458 J60712.AP], 1.5 mL 5M NaCl, 12.5 µL 2M spermidine, 1 Roche c0mplete Protease Inhibitor EDTA-
459 free tablet with ddH2O to 50 mL). 10 µL of solution was taken for counting on the EVE Countess
460 Automated Cell Counter (NanoEntek). After addition of 810 µL of Wash Buffer to resuspend nuclei,

461 100 µL of DMSO [ThermoFisher, 414885000] was added, followed by a brief vortex. Cross-linked
462 microglial nuclei were then placed in a Mr. Frosty (ThermoFisher, 5100-0001) container filled with
463 100% isopropyl alcohol and placed at -80°C until future use.

464 **7.2 Concanavalin A Conjugation:** Magnetic microbeads were conjugated with Concanavalin A
465 (Sigma Aldrich, C2272-10mg) as previously described [72]. Briefly, 50 µL MyOne T1 Streptavidin-
466 conjugated Dynabeads (ThermoFisher, 65601) were placed into a 1.5 mL tube and then placed onto a
467 magnetic stand. The supernatant was removed, and beads were washed three times with 1 X PBS pH 6.8
468 (Sigma Aldrich, 1218-75) while still on the stand. Beads were then resuspended in 50 µL 1 X PBS pH
469 6.8 with 0.01% Tween-20 (Sigma Aldrich, 1003018242). 25 µL of biotin-conjugated Concanavalin A
470 solution (2.3 mg/mL resuspended in 1X PBS pH 6.8 with 0.01% Tween-20) was added to the beads.
471 Beads were incubated at room temperature for 30 minutes with rotation. Beads were placed back onto
472 the magnetic stand and the supernatant was removed. 50 µL of 1X PBS with 0.01% Tween-20 was
473 added to resuspend the beads.

474 **7.3 Bead Activation**: Freshly conjugated beads (3.5 µL per reaction) were immediately added to 1 mL
475 Binding Buffer (200 µL 1M HEPES pH 7.9, 100 µL 1M KCl, 10 µL 1M $CaCl_2$, 10 µL 1M $MnCl_2$
476 [ThermoFisher, J63150.AP] with 9.680 mL ddH2O) and mixed by pipetting. Beads were placed on a
477 magnetic stand and supernatant was removed. Beads were then washed 2x with 300 µL Binding Buffer
478 and mixed by pipetting. After removal of final supernatant, beads were resuspended in total reaction
479 volume (i.e., 45.5 µL for 13 reactions) and left at room temperature until use.

480 **7.4 Cell Preparation and Bead Binding**: Briefly, lightly cross-linked microglial nuclei were placed in
481 room temperature water until completely thawed. Previously obtained nuclei counts were used to
482 estimate the volume of microglial nuclei needed to achieve 2,500 nuclei per reaction (run in duplicate
483 per mark of interest) and was added to individual 0.5 mL thin-walled PCR tubes. While gently
484 vortexing, 3.5 µL of activated beads were added to each tube and incubated for 10 minutes at room
485 temperature with rotation. Following incubation, samples were placed on a magnetic stand and
486 supernatant was removed with repeated draws of a p20 pipette. Bead-bound microglial nuclei were
487 resuspended in 25 µL Antibody Incubation Buffer (995 µL Wash Buffer with 5 µL 200x BSA [B9000S,
488 New England Biolabs]).

489 **7.5 Primary Antibody Binding and Spike-In Preparation**: Lysine-Methyl Panel Spike in (SNAP-
490 CUTANA™ K-MetStat Panel, 19-1002, Epicypher) was diluted 1:10 in Antibody Incubation Buffer.
491 Prior to antibody addition, 0.75 µL of 1:10 spike in panel was added to each reaction. Following this
492 addition, 1 µL of Rabbit anti-H3K27me3 (9733S, CST), 1.5 µL of Rabbit anti-H3K27ac (8173S, CST),
493 or 1.5 µL Rabbit (DA1E) mAb IgG (66362S, CST) antibody was added to each reaction. Samples were
494 incubated for 2 hours at room temperature on a belly dancer (BenchWaver™ 3D Rocker, Benchmark
495 Scientific) (105 RPM) and then transferred to 4°C for overnight incubation without rotation.

496 **7.6 Secondary and pAG-TN5 Incubation:** Samples were removed from 4°C for at least 30 minutes
497 prior to use and then resuspended using light vortexing before placing onto magnetic stand. Supernatant
498 was removed and 25 µL of secondary antibody solution was added to each reaction (Guinea Pig Anti-
499 Rabbit: 1:100 in Wash Buffer, ABIN101961, Antibodies Online) while gently vortexing, then incubated
500 for 1 hour at room temperature on a belly dancer (105 RPM). Samples were then placed on a magnetic
501 stand, supernatant removed and 200 µL Wash Buffer added without disturbing the beads. 185 µL Wash

502 Buffer was removed, and samples spun down, followed by final liquid removal using a p20 pipette. 25
503 µL of pAG-TN5 adaptor complex (1:20, CUTANA™ pAG-Tn5 for CUT&Tag, 15-1017, Epicypher) in
504 300-Wash Buffer (1 mL 1M HEPES pH 7.5, 3 mL 5M NaCl, 12.5 µL 2M spermidine, and 1 Roche
505 c0mplete Protease Inhibitor EDTA-free tablet with ddH2O to 50 mL) was squirted onto beads. Gently
506 vortexing and/or tube rocking was used to ensure all beads were in solution prior to incubation for 2
507 hours at room temperature on a belly dancer (105 RPM).

508 **7.7 Tagmentation:** Following incubation with pAG-TN5, samples were placed back onto magnetic
509 stand and washed with 300-Wash Buffer as described previously. While taking care to avoid beads
510 drying out, 50 µL Tagmentation Buffer (990 µL 300-Wash Buffer with 10 µL 1M MgCl$_2$ [Invitrogen,
511 AM9530G]) was added to each tube. Tubes were lightly rocked to resuspend all beads into solution
512 followed by a brief spin-down. Samples were then incubated for 1 hour at 37°C on a thermal cycler with
513 a hold at 8°C.

514 **7.8 Chromatin Release, Amplification and Clean-up:** Samples were allowed to warm to room
515 temperature and were gently vortexed to resuspend beads before placing back onto magnetic stand.
516 Tagmentation Buffer was withdrawn with subsequent draws from a p20 pipette, and samples were
517 resuspended in 50 µL TAPS Wash Buffer (30 µL 1M TAPS pH 8.5 [BostonBio Products, BB-2375], 1.2
518 µL 0.5M EDTA [Invitrogen, AM9262] and filled to 3 mL with ddH2O) and gently rocked to resuspend
519 beads. Samples were placed back on magnetic stand and buffer was removed following the previous
520 method one sample at a time. After all liquid was removed, samples were resuspended in 5 µL SDS-
521 Release Solution (10 µL 10% SDS [ThermoFisher, 15553027], 10 µL 1M TAPS pH 6.8 and 980 µL
522 ddH2O). A p10 pipette tip was used to drag the solution around the sides of the tubes to grab remaining
523 beads and samples were spun down before being incubated on a thermocycler set to 58°C for 1-hour.
524 Samples were then removed from the thermocycler, placed on ice and spiked with 15 µL of Triton
525 Neutralization Solution (67 µL 10% Triton X-100 with 933 µL ddH2O). Samples were vortexed on high
526 and placed back on ice. 2 µL of an i5 (10 µM) and i7 (10 µM) index [73] were then added to each
527 reaction along with 25 µL NEBNext HiFi 2X PCR Master Mix (New England Biolabs, M0541).
528 Samples were again vortexed on full speed for 10 seconds and briefly spun down. PCR was conducted
529 with the following parameters: Step 1 = 58°C for 5 minutes, Step 2 = 72°C for 5 minutes, Step 3 = 98°C
530 for 5 minutes (Cycle time increased from 30 seconds to account for full reversal of cross-linking), Step 4
531 = 98°C for 10 seconds, Step 5 = 60°C for 10 seconds, (Repeat Steps 4-5 14 times), Step 6 = 72°C for 1
532 minute and hold at 8°C. Samples were allowed to warm to room temperature for 30 minutes and then
533 were incubated with 65 µL SPRIselect beads (Beckman Coulter, B23318) (1.3X) for 10 minutes.
534 Samples were then placed onto a magnetic stand and beads were washed twice with 80% freshly made
535 EtOH without removing the tubes from the stand. Samples were spun down following the last wash and
536 placed back onto the stand to remove all traces of EtOH. The purified DNA product was released from
537 the beads by incubating in 17 µL freshly made 10 mM Tris-HCl pH 8.0 (EMD Millipore, 648314-
538 100mL) for 10 minutes. Samples were then placed back onto a magnetic stand and 15 µL of purified
539 product was transferred to barcoded tubes for storage.

540 **7.9 Sample Pooling and DNA Sequencing:** Samples were pooled to equimolar concentrations based on
541 Qubit 1x dsDNA high sensitivity (ThermoFisher, Q33230) concentration and fragment size from the
542 Bioanalyzer HS DNA kit (Agilent, 5067-4626) and sequenced on the Illumina NovaSeq6000 platform
543 (150x150bp PE), targeting 10 million reads per sample by the University of Miami Center John P.
544 Hussman Institute for Human Genomics sequencing core facility.

8. CUT&Tag-Direct Data Processing: CUT&Tag-Direct data used in this study were mapped to the mm10 genome. Prior to mapping, raw sequencing reads were mapped to the genome using Bowtie2 [74] (v. 2.4.5) with the following parameters: --local --very-sensitive --no-mixed --no-discordant --phred33 -I 10 -X 700. Resulting sam files were sorted and duplicates were marked. For control samples, (i.e. IgG targets) duplicates were removed, while remaining samples retained all duplicates. Samtools [75] (v. 1.12) was used to assess fragment length and write uniquely mapped reads from sam files into bam files. Resulting bam files were sorted and indexed. Technical replicates were kept independent and merged using samtools merge followed by sorting and indexing. Bedtools (v 2.30.0) [76] bamtobed function was then used to convert both merged files and independent files to bed files. Resulting bed files were cleaned and fragment columns were extracted using 500bp bins across the genome. These resulting files were used to assess replicate reproducibility via correlation plots. Following visualization, cleaned bed files containing fragments were normalized to barcoded read counts generated from spike-in dNuc's with a constant value of 500,000. Peak calling was conducted using SEACR [44] on normalized bedgraph files for each biological replicate (n=2) against merged IgG controls using the following settings: "non" and "stringent". Resulting significant peaks were used for downstream analyses. Visualization and QC plots were generated in R. All associated code for pre-processing of data files is available upon request.

9 Correlating RNA-sequencing Data with CUT&Tag-Direct Peaks

9.1 Generation of Gene Expression Lists: Fragments Per Kilobase of transcript per Million mapped reads (FPKM) generated using Stringtie (v 2.1.7) [64] during pre-processing from RNA-sequencing data was merged and annotated using biomaRt (v 2.28.0) [77, 78] with ENSMBL ID's. Protein-coding genes were selected and filtered based on expression levels. Genes with > 10 FPKM were subset into a "High Expression" group, genes with $1 < FPKM < 10$ were subset into a "Medium Expression" group and genes with < 1 FPKM were subset into the "Low Expression" group based on brain region.

9.2 Generation of Significant Called Peaks Lists: Significantly called peaks for each brain region and histone mark, based on 2 technical replicates, were annotated using HOMER [79] against the mm10 genome and any peaks mapped to genes that fall within the promoter, promoter-transcriptional-start-site (TSS) or TSS and that were protein-coding were retained for downstream analysis for H3K27ac. The same was conducted for H3K27me3 peaks, however peaks falling into an exon of these genes were also included. Fragment counts from associated bam files were used to count fragments in significantly called peaks to generate peak expression matrices for use with DESeq2.

9.3 Gene Overlap The R package GeneOverlap (v1.30.0) [80] was then used to conduct statistical overlap testing of highly expressed genes, medium expressed genes and lowly expressed genes with the presence of significant peak calls in such regions for both H3K27ac and H3K27me3. Odds ratios were used to generate intersection lists of significantly associated peaks with gene expression for further analysis. Peaks found to overlap with gene expression in both replicates were retained. To determine the epigenetic identities specific to each region, peaks found to overlap with expression in the same genes in more than one region were removed, leaving behind only those specific to one region of the brain. GO analysis was then conducted on these genes using methods described above to determine the distinct features of epigenetic regulation in each region and the rrvgo package [68] was utilized to reduce GO terms to parent terms for clarity. To generate significant overlaps between significant gene expression and significantly correlated epigenetic features, the lists of significantly differentially expressed genes

587   with a positive or negative $\log_2$FC from DESeq2 conducted on RNA-sequencing data sets was taken and
588   compared to peaks meeting the criteria as described above for highly expressed genes and presence of
589   H3K27ac peaks, and downregulated genes and the presence of H3K27me3 peaks. The number of genes
590   intersecting were used to generate representative Venn diagrams. All protein coding genes mapped were
591   used as background for gene overlap.

592   **9.4 Visualization of Overlapping CUT&Tag-Direct/RNA-sequencing data:** Bam files generated
593   from mapped read alignments for both RNA-sequencing and CUT&Tag-Direct sequencing data were
594   used to generate bigWig files for visualization. Samples 7 and 8 from RNA-sequencing data were used
595   as input as they correspond to the same animals and regions used for CUT&Tag-Direct data. Using
596   deepTools [81] bamCoverage, bam files from CUT&Tag-Direct sequencing were screened against
597   blacklisted regions [82] and converted to bigWig files using the following parameters: --binSize 10, --
598   normalizeUsing RPCG – effectiveGenomeSize 2652783500 –ignoreForNormalization chrX and --
599   extendReads. Following conversion, bigWig files from biological replicates were merged using
600   bigWigMerge from the UCSC genome browser bwtools. Merged files were sorted and then converted
601   back into bigWigs using the bedgraphToBigWig program [83]. For RNA-sequencing data, using
602   deepTools [81] bamCoverage, bam files were normalized for read coverage using the inverse scale
603   factors calculated by DESeq2 and converted to bigWig files using the following parameters: --binSize 1
604   and --skipNonCoveredRegions. Following conversion, bigWig files from biological replicates were
605   merged using bigWigMerge from bwtools. Merged files were sorted and then converted back into
606   bigWigs using the bedgraphToBigWig program [83]. The resulting bigWig files were visualized using
607   rtracklayer (v 1.58.0) [84], TrackPlotR (v. 0.0.1) [85] and ggplot2 (v. 3.5.0.9000).

608   **10. Statistical Analysis:** Statistical analyses were conducted in accordance with the various packages
609   used for RNA-sequencing data as well as CUT&Tag-Direct data. Information on specific analyses run
610   can be found in the associated code and methods sections.

References

613   1.   Polazzi, E. and B. Monti, *Microglia and neuroprotection: from in vitro studies to therapeutic*
614   *applications.* Prog Neurobiol, 2010. **92**(3): p. 293-315.
615   2.   Chen, Z. and B.D. Trapp, *Microglia and neuroprotection.* J Neurochem, 2016. **136 Suppl 1**: p. 10-
616   7.
617   3.   Barko, K., et al., *Brain region- and sex-specific transcriptional profiles of microglia.* Front
618   Psychiatry, 2022. **13**: p. 945548.
619   4.   Tan, Y.L., Y. Yuan, and L. Tian, *Microglial regional heterogeneity and its role in the brain.* Mol
620   Psychiatry, 2020. **25**(2): p. 351-367.
621   5.   Masuda, T., et al., *Microglia Heterogeneity in the Single-Cell Era.* Cell Rep, 2020. **30**(5): p. 1271-
622   1281.
623   6.   De Biase, L.M., et al., *Local Cues Establish and Maintain Region-Specific Phenotypes of Basal*
624   *Ganglia Microglia.* Neuron, 2017. **95**(2): p. 341-356 e6.
625   7.   Tarozzo, G., et al., *Fractalkine protein localization and gene expression in mouse brain.* J
626   Neurosci Res, 2003. **73**(1): p. 81-8.
627   8.   Bottcher, C., et al., *Human microglia regional heterogeneity and phenotypes determined by*
628   *multiplexed single-cell mass cytometry.* Nat Neurosci, 2019. **22**(1): p. 78-90.
629   9.   Grabert, K., et al., *Microglial brain region-dependent diversity and selective regional sensitivities*
630   *to aging.* Nat Neurosci, 2016. **19**(3): p. 504-16.

10. Yeh, H. and T. Ikezu, *Transcriptional and epigenetic regulation of microglia in health and disease.* Trends Mol Med, 2019. **25**(2): p. 96-111.

11. Ayata, P., et al., *Epigenetic regulation of brain region-specific microglia clearance activity.* Nat Neurosci, 2018. **21**(8): p. 1049-1060.

12. Martins-Ferreira, R., et al., *Microglial innate memory and epigenetic reprogramming in neurological disorders.* Prog Neurobiol, 2021. **200**: p. 101971.

13. Kierdorf, K., et al., *Microglia emerge from erythromyeloid precursors via Pu.1- and Irf8-dependent pathways.* Nat Neurosci, 2013. **16**(3): p. 273-80.

14. Nott, A., et al., *Brain cell type-specific enhancer-promoter interactome maps and disease-risk association.* Science, 2019. **366**(6469): p. 1134-1139.

15. Scholz, R., et al., *Epigenetic control of microglial immune responses.* Immunol Rev, 2024. **323**(1): p. 209-226.

16. Troutman, T.D., E. Kofman, and C.K. Glass, *Exploiting dynamic enhancer landscapes to decode macrophage and microglia phenotypes in health and disease.* Mol Cell, 2021. **81**(19): p. 3888-3903.

17. Russo, S.J. and E.J. Nestler, *The brain reward circuitry in mood disorders.* Nat Rev Neurosci, 2013. **14**(9): p. 609-25.

18. Dichter, G.S., C.A. Damiano, and J.A. Allen, *Reward circuitry dysfunction in psychiatric and neurodevelopmental disorders and genetic syndromes: animal models and clinical findings.* J Neurodev Disord, 2012. **4**(1): p. 19.

19. Perry, D.C. and J.H. Kramer, *Reward processing in neurodegenerative disease.* Neurocase, 2015. **21**(1): p. 120-33.

20. Keren-Shaul, H., et al., *A Unique Microglia Type Associated with Restricting Development of Alzheimer's Disease.* Cell, 2017. **169**(7): p. 1276-1290 e17.

21. Holtman, I.R., et al., *Induction of a common microglia gene expression signature by aging and neurodegenerative conditions: a co-expression meta-analysis.* Acta Neuropathol Commun, 2015. **3**: p. 31.

22. Koskuvi, M., et al., *Genetic contribution to microglial activation in schizophrenia.* Mol Psychiatry, 2024.

23. Vilca, S.J., et al., *Transcriptional and epigenetic regulation of microglia in substance use disorders.* Mol Cell Neurosci, 2023. **125**: p. 103838.

24. Johnstone, A.L., et al., *Dysregulation of the histone demethylase KDM6B in alcohol dependence is associated with epigenetic regulation of inflammatory signaling pathways.* Addict Biol, 2021. **26**(1): p. e12816.

25. Zhang, X., et al., *Epigenetic regulation of innate immune memory in microglia*. 2022, BioMed Central. p. 1-19.

26. Chastain, L.G., et al., *Early life alcohol exposure primes hypothalamic microglia to later-life hypersensitivity to immune stress: possible epigenetic mechanism.* Neuropsychopharmacology, 2019. **44**(9): p. 1579-1588.

27. Das, A., et al., *Transcriptome sequencing of microglial cells stimulated with TLR3 and TLR4 ligands.* BMC Genomics, 2015. **16**: p. 517.

28. Cheray, M. and B. Joseph, *Epigenetics control microglia plasticity.* Front Cell Neurosci, 2018. **12**: p. 243.

29. Fujita, Y., T. Yamashita, and *Alterations in Chromatin Structure and Function in the Microglia*. 2021. p. 1-13.

30. Huang, M., et al., *Microglial immune regulation by epigenetic reprogramming through histone H3K27 acetylation in neuroinflammation.* Front Immunol, 2023. **14**: p. 1052925.

31. Meleady, L., et al., *Histone deacetylase 3 regulates microglial function through histone deacetylation.* Epigenetics, 2023. **18**(1): p. 2241008.

32. Crapser, J.D., et al., *Microglia as hackers of the matrix: sculpting synapses and the extracellular space.* Cell Mol Immunol, 2021. **18**(11): p. 2472-2488.

33. Nguyen, P.T., et al., *Microglial Remodeling of the Extracellular Matrix Promotes Synapse Plasticity.* Cell, 2020. **182**(2): p. 388-403 e15.

34. Gray, D.T., et al., *Microglia promote extracellular matrix deposition and restrict excitatory synapse numbers*

in the mesolimbic dopamine system during healthy aging. BioRxiv, 2024.

35. Yeo, S., et al., *Primary cilia-mediated regulation of microglial secretion in Alzheimer's disease.* Front Mol Biosci, 2023. **10**: p. 1250335.

36. Garay, P.A., et al., *Maternal immune activation causes age- and region-specific changes in brain cytokines in offspring throughout development.* Brain Behav Immun, 2013. **31**: p. 54-68.

37. Badimon, A., et al., *Negative feedback control of neuronal activity by microglia.* Nature, 2020. **586**(7829): p. 417-423.

38. Pike, A.F., et al., *Dopamine signaling modulates microglial NLRP3 inflammasome activation: implications for Parkinson's disease.* J Neuroinflammation, 2022. **19**(1): p. 50.

39. Kopec, A.M., et al., *Microglial dopamine receptor elimination defines sex-specific nucleus accumbens development and social behavior in adolescent rats.* Nat Commun, 2018. **9**(1): p. 3769.

40. Cai, Y., et al., *H3K27me3-rich genomic regions can function as silencers to repress gene expression via chromatin interactions.* Nat Commun, 2021. **12**(1): p. 719.

41. Cao, R., et al., *Role of histone H3 lysine 27 methylation in Polycomb-group silencing.* Science, 2002. **298**(5595): p. 1039-43.

42. Creyghton, M.P., et al., *Histone H3K27ac separates active from poised enhancers and predicts developmental state.* Proc Natl Acad Sci U S A, 2010. **107**(50): p. 21931-6.

43. Henikoff, S., et al., *Efficient chromatin accessibility mapping in situ by nucleosome-tethered tagmentation.* Elife, 2020. **9**.

44. Meers, M.P., D. Tenenbaum, and S. Henikoff, *Peak calling by Sparse Enrichment Analysis for CUT&RUN chromatin profiling.* Epigenetics Chromatin, 2019. **12**(1): p. 42.

45. Lavarone, E., C.M. Barbieri, and D. Pasini, *Dissecting the role of H3K27 acetylation and methylation in PRC2 mediated control of cellular identity.* Nat Commun, 2019. **10**(1): p. 1679.

46. Zhao, W., et al., *Investigating crosstalk between H3K27 acetylation and H3K4 trimethylation in CRISPR/dCas-based epigenome editing and gene activation.* Sci Rep, 2021. **11**(1): p. 15912.

47. Butovsky, O. and H.L. Weiner, *Microglial signatures and their role in health and disease.* Nat Rev Neurosci, 2018. **19**(10): p. 622-635.

48. Chung, H.Y., et al., *Microglia mediate neurocognitive deficits by eliminating C1q-tagged synapses in sepsis-associated encephalopathy.* Sci Adv, 2023. **9**(21): p. eabq7806.

49. Moca, E.N., et al., *Microglia Drive Pockets of Neuroinflammation in Middle Age.* J Neurosci, 2022. **42**(19): p. 3896-3918.

50. Uriarte Huarte, O., et al., *Single-Cell Transcriptomics and In Situ Morphological Analyses Reveal Microglia Heterogeneity Across the Nigrostriatal Pathway.* Front Immunol, 2021. **12**: p. 639613.

51. Masuda, T., et al., *Spatial and temporal heterogeneity of mouse and human microglia at single-cell resolution.* Nature, 2019. **566**(7744): p. 388-392.

52. Gerrits, E., et al., *Transcriptional profiling of microglia; current state of the art and future perspectives.* Glia, 2020. **68**(4): p. 740-755.

53. Hammond, T.R., et al., *Single-cell RNA sequencing of microglia throughout the mouse lifespan and in the injured brain reveals complex cell-state changes.* Immunity, 2019. **50**(1): p. 253-271 e6.

54. Matcovitch-Natan, O., et al., *Microglia development follows a stepwise program to regulate brain homeostasis.* Science, 2016. **353**(6301): p. aad8670.

55. Van Hove, H., et al., *A single-cell atlas of mouse brain macrophages reveals unique transcriptional identities shaped by ontogeny and tissue environment.* Nat Neurosci, 2019. **22**(6): p. 1021-1035.

732 56. Kosoy, R., et al., *Genetics of the human microglia regulome refines Alzheimer's disease risk loci.*
733   Nat Genet, 2022. **54**(8): p. 1145-1154.
734 57. Achiro, J.M., et al., *Aging differentially alters the transcriptome and landscape of chromatin*
735   *accessibility in the male and female mouse hippocampus.* Front Mol Neurosci, 2024. **17**: p.
736   1334862.
737 58. Conway, E., E. Healy, and A.P. Bracken, *PRC2 mediated H3K27 methylations in cellular identity*
738   *and cancer.* Curr Opin Cell Biol, 2015. **37**: p. 42-8.
739 59. McCarthy, M.M., B.M. Nugent, and K.M. Lenz, *Neuroimmunology and neuroepigenetics in the*
740   *establishment of sex differences in the brain.* Nat Rev Neurosci, 2017. **18**(8): p. 471-484.
741 60. Osborne, B.F., A. Turano, and J.M. Schwarz, *Sex Differences in the Neuroimmune System.* Curr
742   Opin Behav Sci, 2018. **23**: p. 118-123.
743 61. Felix Krueger, F.J., Phil Ewels, Ebrahim Afyounian, Michael Weinstein, Benjamin Schuster-
744   Boeckler, Gert Hulselmans, & sclamons, *TrimGalore: v0.6.10 - add default decompression path*
745   *(0.6.10).* 2023: Zenodo.
746 62. Martin, M., *Cutadapt removes adapter sequences from high-throughput sequencing reads.*
747   EMBnet.journal, 2011. **17**(1): p. 10-12.
748 63. Dobin, A., et al., *STAR: ultrafast universal RNA-seq aligner.* Bioinformatics, 2013. **29**(1): p. 15-
749   21.
750 64. Pertea, M., et al., *StringTie enables improved reconstruction of a transcriptome from RNA-seq*
751   *reads.* Nat Biotechnol, 2015. **33**(3): p. 290-5.
752 65. Love, M.I., W. Huber, and S. Anders, *Moderated estimation of fold change and dispersion for*
753   *RNA-seq data with DESeq2.* Genome Biol, 2014. **15**(12): p. 550.
754 66. Wu, T., et al., *clusterProfiler 4.0: A universal enrichment tool for interpreting omics data.*
755   Innovation (Camb), 2021. **2**(3): p. 100141.
756 67. Yu, G., et al., *clusterProfiler: an R package for comparing biological themes among gene clusters.*
757   OMICS, 2012. **16**(5): p. 284-7.
758 68. Sayols, S., *rrvgo: a Bioconductor package for interpreting lists of Gene Ontology terms.* MicroPubl
759   Biol, 2023. **2023**.
760 69. Langfelder, P. and S. Horvath, *WGCNA: an R package for weighted correlation network analysis.*
761   BMC Bioinformatics, 2008. **9**: p. 559.
762 70. Ritchie, M.E., et al., *limma powers differential expression analyses for RNA-sequencing and*
763   *microarray studies.* Nucleic Acids Res, 2015. **43**(7): p. e47.
764 71. Steven Henikoff, J.H., Kami Ahmad, *CUT&Tag-direct for whole cells with CUTAC.* protocols.io,
765   2023. **4**.
766 72. Fujiwara, Y., et al., *Preparation of optimized concanavalin A-conjugated Dynabeads(R) magnetic*
767   *beads for CUT&Tag.* PLoS One, 2021. **16**(11): p. e0259846.
768 73. Buenrostro, J.D., et al., *Single-cell chromatin accessibility reveals principles of regulatory*
769   *variation.* Nature, 2015. **523**(7561): p. 486-90.
770 74. Langmead, B. and S.L. Salzberg, *Fast gapped-read alignment with Bowtie 2.* Nat Methods, 2012.
771   **9**(4): p. 357-9.
772 75. Danecek, P., et al., *Twelve years of SAMtools and BCFtools.* Gigascience, 2021. **10**(2).
773 76. Quinlan, A.R. and I.M. Hall, *BEDTools: a flexible suite of utilities for comparing genomic features.*
774   Bioinformatics, 2010. **26**(6): p. 841-2.
775 77. Durinck, S., et al., *Mapping identifiers for the integration of genomic datasets with the*
776   *R/Bioconductor package biomaRt.* Nature Protocols, 2009. **4**(8): p. 1184-1191.
777 78. Durinck, S., et al., *BioMart and Bioconductor: a powerful link between biological databases and*
778   *microarray data analysis.* Bioinformatics, 2005. **21**(16): p. 3439-40.
779 79. Heinz, S., et al., *Simple combinations of lineage-determining transcription factors prime cis-*
780   *regulatory elements required for macrophage and B cell identities.* Mol Cell, 2010. **38**(4): p. 576-
781   89.
782 80. Shen L, S., *GeneOverlap: Test and visualize gene overlaps.* 2024: Bioconductor.

81. Ramirez, F., et al., *deepTools2: a next generation web server for deep-sequencing data analysis.* Nucleic Acids Res, 2016. **44**(W1): p. W160-5.
82. Amemiya, H.M., A. Kundaje, and A.P. Boyle, *The ENCODE Blacklist: Identification of Problematic Regions of the Genome.* Sci Rep, 2019. **9**(1): p. 9354.
83. Kent, W.J., et al., *BigWig and BigBed: enabling browsing of large distributed datasets.* Bioinformatics, 2010. **26**(17): p. 2204-7.
84. Lawrence, M., R. Gentleman, and V. Carey, *rtracklayer: an R package for interfacing with genome browsers.* Bioinformatics, 2009. **25**(14): p. 1841-2.
85. Mayakonda, A. and F. Westermann, *Trackplot: a fast and lightweight R script for epigenomic enrichment plots.* Bioinform Adv, 2024. **4**(1): p. vbae031.

Author contributions:

Conceptualization: AVM, SJV, LMT

Methodology: AVM, SJV, FBG, LMT

Software: AVM

Investigation: AVM, SJV, LMT

Visualization: AVM, SJV

Data Curation: AVM, SJV

Supervision: FBG, LMT

Writing—original draft: AVM, SJV, LMT

Writing—review & editing: AVM, SJV, LMT

Competing interests:

The authors declare that they have no known competing financial interests or personal relationships that could have appeared to influence the work reported in this paper.

Data and materials availability:

All next generation sequencing files associated with this study as well as the code that was used to pre-process and run differential expression are available online at https://github.com/avm27/RegionalMicroglialTranscriptomicsandEpigenomics. All data files used in processing and analysis will be available from the GEO/SRA following publication and/or upon request.